Reduction in Tension and Stiffening of Lipid Membranes in an Electric Field Revealed by X-ray Scattering

Arnaud Hemmerle and Thierry Charitat*

*UPR 22/CNRS, Institut Charles Sadron, Université de Strasbourg,
23 rue du Loess, BP 84047 67034 Strasbourg Cedex 2, France*

Giovanna Fragneto

Institut Laue-Langevin, 71 av. des Martyrs, BP 156, 38042 Grenoble Cedex, France

Jean Daillant

Synchrotron SOLEIL, L'Orme des Merisiers, Saint-Aubin, BP 48, F-91192 Gif-sur-Yvette Cedex, France
(Dated: January 5, 2016)

The effect of AC electric fields on the elasticity of supported lipid bilayers has been investigated at the microscopic level using grazing incidence synchrotron x-ray scattering. A strong decrease in the membrane tension up to 1mN/m and a dramatic increase of its effective rigidity up to $300k_BT$ are observed for local electric potentials seen by the membrane $\lesssim$ 1V. The experimental results were analyzed using detailed electrokinetic modeling and non-linear Poisson-Boltzmann theory. Analysis of electrostriction effects demonstrates an accurate modeling of the electromagnetic stress. Accurate modeling of our data shows that the decrease in tension results from the amplification of charge fluctuations on the membrane surface whereas the increase in bending rigidity results from effects in the electric double layer. These effects eventually lead to a destabilization of the bilayer and vesicle formation. Similar effects are expected at the tens of nanometer lengthscale in cell membranes with lower tension, and could explain a number of electrically driven processes.

Electric fields can be used to destabilize lipid bilayers as in the electroformation process, the most popular method to form large unilamellar vesicles [1], or to manipulate the shape of vesicles [2–4]. Beyond biosensor applications and the investigation of fundamental mechanical, dynamical and binding properties of membranes using impedance spectroscopy or dielectric relaxation [5], the strong influence of electric fields on lipid membrane behavior is also used in numerous applications in cell biology, biotechnology and pharmacology [6, 7] such as cell hybridization [8], electroporation [9], electrofusion [10] and electropermeabilization [11]. All these effects imply a strong deformation of the membranes in the field, the understanding of which in terms of elastic properties is therefore of prime importance [12]. Theoretically, the effect of electric fields on membrane tension has been investigated in Ref. [13], which was extended to bending rigidity in Refs [14, 15].

When placed in an electric field **E**, charges of opposite sign will accumulate at both sides of a membrane which can be seen as a capacitor. For a flat membrane, a direct consequence is electrostriction: at equilibrium, the elastic response of the membrane balances the electrostatic pressure [16]. Beyond this simple effect, membrane fluctuations modify the boundary conditions for the electric field, leading to a subtle coupling between electrostatics and membrane elasticity. The sur-

face charge density excess for a surface mode $z_q \exp(i\mathbf{q}.\mathbf{r})$ is $\sigma_m = -\epsilon_m E_m d_m q^2 \exp(i\mathbf{q}.\mathbf{r})$, where ϵ_m and d_m are the membrane permittivity and thickness, E_m the field seen by the membrane, and $q^2 z_q$ the local curvature. The work of the electric field to reach this configuration is $\sigma_m E_m z_q \exp(i\mathbf{q}.\mathbf{r})$. As $q^2 z_q^2$ is the increase in area of the fluctuating membrane, this means that there is a negative correction to the free energy $\propto q^2 E_m^2$, i.e. a negative (destabilizing) contribution Γ_m to the membrane surface tension γ [13]. Similar effects occur in the electric double layer leading to a total correction $\Gamma_{el} = \Gamma_m + \Gamma_{DL}$, where Γ_{DL} is the usually smaller correction coming from the electrical double layer [14]. Taking into account non-linear effects in the electric double layer we have,

$$\Gamma_m = -\epsilon_m d_m E_m^2 = -\frac{\epsilon_m}{d_m}\left[V_{loc} - \frac{4k_BT}{e}\ln\left(\frac{1+c}{1-c}\right)\right]^2, \quad (1)$$

where V_{loc} is the local electric potential seen by the bilayer and the double electric layer, lower than the applied potential. $0 < c < 1$ is a dimensionless parameter depending on Debye screening length κ_D and voltage, saturating to 1 for either high salt or high voltage because of non-linear effects in the Debye layer [14, 17]. Further development in powers of q give contributions in q^4 [4, 14], corresponding to a positive correction $K_{el} = K_m + K_{DL}$ to the membrane bending rigidity κ, where the largest correction is now due to the double layer:

$$K_{DL} = 4\epsilon_w\left(\frac{k_BT}{e}\right)^2 \kappa_D^{-1}\frac{c^2(3-c^2)}{1+c^2}, \quad (2)$$
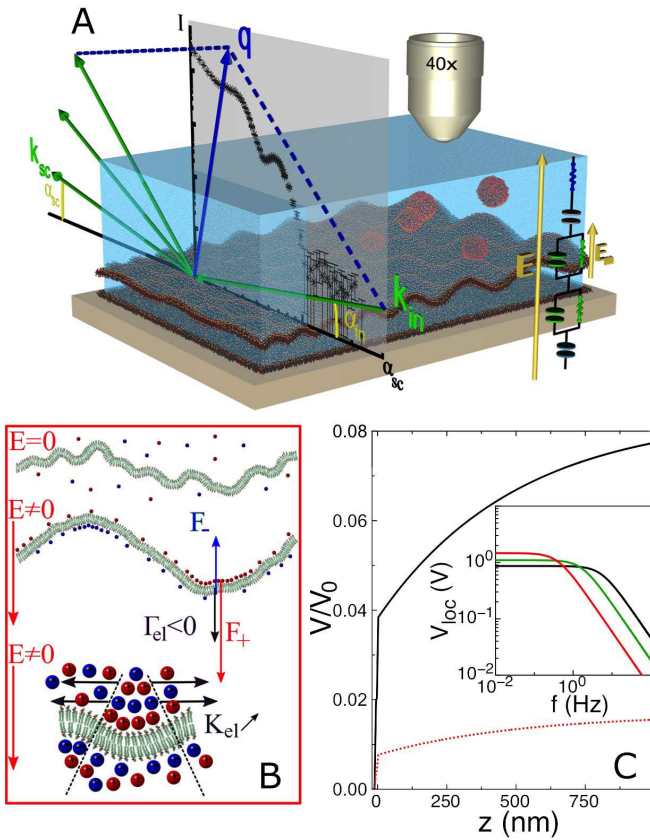
where ϵ_w is the permittivity of water.

FIG. 1: Schematic view of the experiment and electokinetic model of the supported bilayers (A). The incident beam at grazing incidence (direction $\mathbf{k_{in}}$) is scattered in direction $\mathbf{k_{sc}}$, giving access to in-plane fluctuations. Schematic representation of the effect of electric field (B). Top, freely fluctuating membrane. Middle, decrease in surface tension induced by the electric field is effective at large length scales. Bottom, increase in bending rigidity, mainly effective at small length scales. Calculated electric potential as a function of the distance from the wall for 10 Hz (black solid curve) and 50 Hz (red dotted line) frequencies (C). The inset of (C) shows the local voltage at the membrane boundaries as a function of frequency and for different Debye lengths $\kappa_D^{-1} = 800$ nm (red curve), $\kappa_D^{-1} = 300$ nm (green curve) and $\kappa_D^{-1} = 150$ nm (black curve).

The model system we have used consisted of two supported bilayers of DSPC ($L-\alpha$ 1,2-distearoyl-sn-glycero-3-phosphocholine, Avanti Polar Lipids, Lancaster, Alabama) deposited on ultra-flat silicon substrates. The first bilayer serves as a spacer to reduce the interaction between the floating second bilayer and the substrate and keep it free to fluctuate [18]. Potential was applied between a Cu layer deposited at the back of the thick Si substrate and an ITO coated glass plate mounted parallel to the substrate in the solution, 0.5 cm from the membrane (Fig. 1.A).

We used a 27 keV x-ray beam (wavelength $\lambda = 0.0459$ nm) at the CRG-IF beamline of the European Synchrotron Radiation Facility (ESRF) in an off-specular ge-

ometry described in Fig. 1.A [19]. Off-specular scattering is sensitive to both static deformation and thermal fluctuations of bilayers. In the limit of small amplitudes, and the simple case of a single bilayer in an interaction potential U, the scattered intensity is $I_{sc} \propto \langle z_q z_{-q} \rangle$, with the fluctuation spectrum $\langle z_q z_{-q} \rangle = k_B T / h(\mathbf{q})$ and

$$h(\mathbf{q}) = U'' + \gamma q^2 + \kappa q^4. \qquad (3)$$

The Hamiltonian of the system is given by $\mathcal{H} = \sum_q \mathcal{H}(\mathbf{q}) = \sum_q h(\mathbf{q}) |z_q|^2$. Fitting of the scattering curves following the procedure of [18, 20] therefore gives access to the bilayer electron density profile, γ, κ and U''. Different scattering curves are presented in Supplemental Material, showing that high voltage differences, up to 10 V can be applied to the cell without destroying the membrane, but strongly affecting its fluctuations. Fig. 2 summarizes the main findings of this paper. First, we clearly observe an electrostriction effect on structural properties. The thickness d_w of water layer in between the two lipid bilayers decreases with the electric field (Fig. 2.A). Depending on voltage and frequency, we also observe large negative corrections to the tension $\Gamma_{el} = \gamma_{(V=0)} - \gamma$ (up to 1 mN/m, Fig. 2.C,D) and positive corrections to the bending stiffness $K_{el} = \kappa - \kappa_{(V=0)}$ (up to a few hundreds of $k_B T$, Fig. 2.E,F).

Analyzing our results first requires to determine the local voltage drop V_{loc} seen by the bilayer. To this end, we model the system electrokinetics by solving the Poisson-Nernst-Planck equations, generalizing the model of Ziebert et al [15] to the double supported bilayer (Fig. 1.A) [17]. The only unknown parameter is the Debye screening length κ_D^{-1}, which might slightly depend on the dissolved carbon dioxide and fixes the conductivity of the solution [21]. Whereas $\kappa_D^{-1} = 960$ nm in pure water, it is reduced to 150 nm for normal atmospheric conditions. As scattering curves were recorded 5 to 10 hours after sample preparation, which can influence the Debye length, $\kappa_D^{-1} = 150$ nm, 300 nm and 800 nm were used in the analysis. With these values and a single diffusion coefficient $D = 7.5 \times 10^{-9}$ m^2/s for all ions [22], the effective membrane resistivity, lower than its intrinsic resistivity, ranges from 20 Ω.cm^2 to 300 Ω.cm^2. The system behaves as a low-pass filter with a cut-off frequency determined by the bulk solution conductance R_B^{-1} and the electric double layer capacitance per unit area C_{DL} (inset of Fig. 1.C), the highest resistance and capacitance in the system respectively. Depending on Debye length, $R_B = 0.5 - 10$ MΩ.cm^2 and $C_{DL} = 0.04 - 0.18$ μF/cm^2, leading to cutoff frequencies of 0.2 Hz for $\kappa_D^{-1} = 150$ nm to 3 Hz for $\kappa_D^{-1} = 800$ nm. Accordingly, the voltage drop at the membrane increases from less than $0.01 V_0$ at 50 Hz to $\approx 0.04 V_0$ at 10 Hz, where V_0 is the AC field applied to the membrane (Fig. 1.C).

First discussing electrostriction, the most compressible part in the system is the water layer in between the two
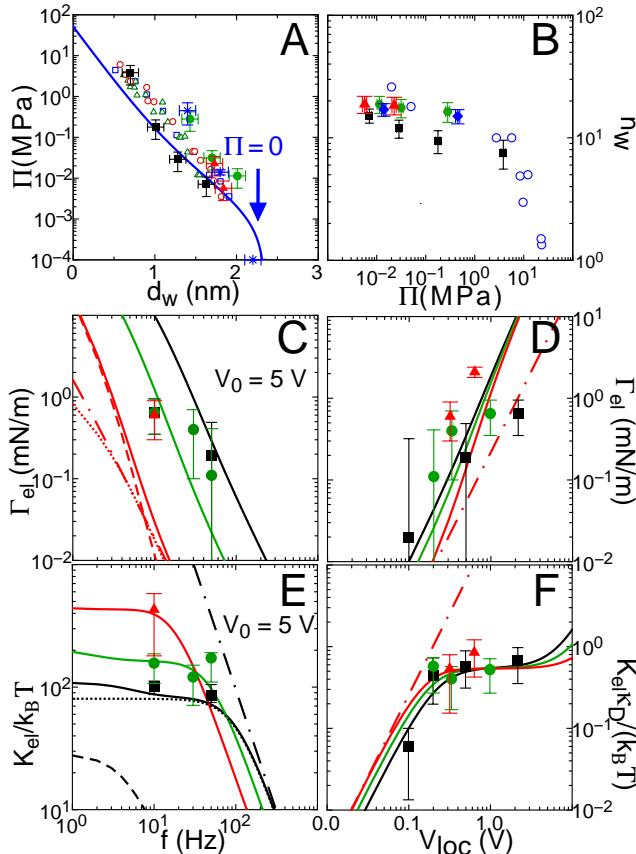
FIG. 2: Effect of an AC field on a supported bilayer. Filled symbols are data from this work. Black squares (■), green circles (●) and red triangles (▲) correspond to different experiments. Solid lines correspond to the full electrostatic contribution (Poisson-Boltzmann) to Γ_{el} and K_{el} which can be decomposed in a membrane contribution (dotted line) and an electric double layer contribution (dashed line). Linear Debye-Hückel theory is shown as dashed-dotted lines. $\kappa_D^{-1} = 800$ nm (red curves), $\kappa_D^{-1} = 300$ nm (green curves) and $\kappa_D^{-1} = 150$ nm (black curves). Mechanical pressure as a function of distance (A). Blue stars are from Ref. [18] where pressure was applied by osmotic stress on similar double bilayers. Empty symbols are from Ref. [23] (osmotic stress on multilayer stacks). The solid line is calculated after Ref. [18] using dispersive, electrostatic and entropic contributions to the inter-bilayer potential. Number of water molecules per lipid n_w as a function of electrostatic pressure Π (B). Blue circles (○) were obtained by NMR spectroscopy for osmotically stressed DMPC multilayer stacks[24]. Electrostatic contribution to the membrane tension Γ_{el} as a function of frequency for a fixed voltage $V_0 = 5$ V (C) and as a function of the local voltage V_{loc} at the membrane (D). Electrostatic contribution to the membrane rigidity K_{el} as a function of frequency for a fixed voltage $V_0 = 5$ V (E) and $K_{el}\kappa_D/k_BT$ as a function of the local potential difference V_{loc} (F).

lipid bilayers and the electromagnetic stress is balanced by the interbilayer potential. By plotting the electrostatic pressure Π [17] as a function of the interbilayer water thickness d_w (Fig. 2.A), all points fall on a master curve obtained for both the natural entropic repulsion between bilayers [18] and osmotic stress, either applied on floating bilayers [18] or multilayer stacks [23], demonstrating that the local electromagnetic stress is well described by our model. We also report in Fig. 2.B the number of water molecules per lipids n_w as a function of the pressure Π. Similar curves obtained when the pressure is osmotically applied on a floating bilayer [18] and on multilayer stacks [24] are also presented, clearly demonstrating that the floating bilayers behave the same way irrespective of how the mechanical stress is applied and keep their integrity under the applied electric field.

The frequency dependence of the correction to the membrane tension Γ_{el} is plotted in Fig. 2.C for $V_0 = 5$ V, where a $\approx \omega^{-2}$ decay is observed. The origin of this purely electrokinetic effect lies in the impossibility to charge the membrane above the cutoff frequency of the low bandpass filter formed by the electric double layer capacitor and bulk water resistor due to the finite mobility of ions in water. By plotting Γ_{el} as a function of the local electric field V_{loc}, we observe a good agreement between data and theoretical predictions with Γ_{el} exhibiting a roughly $\propto V_{loc}^2$ dependence (Fig. 2D).

The increase in bending rigidity of the membrane K_{el} is plotted as a function of frequency for $V_0 = 5$ V in Fig. 2.E and as a function of V_{loc} in Fig. 2.F. Both curves exhibit a more complex behavior than the Γ_{el} curves which can be attributed to non-linear effects due to the large voltage drop at the membrane with $eV/k_BT \simeq 1$ (Fig. 1.C). In contrast with the linear theory which exhibits the expected ω^{-2} behavior, the low-frequency plateau seen for both experimental data and non-linear theory in Fig. 2.E comes from saturation effects in the electric double layer. By plotting the data as a function of V_{loc}, which allows one to decouple microscopic and electrokinetic effects, all $K_{el}\kappa_D$ values indeed fall on a master curve with a saturation from 0.5V (see Fig. 2.F). This is in remarkable agreement with the theory which predicts a saturation value of K_{el} proportional to the Debye length [15], and fully consistent with the expectation that a thicker layer is more difficult to bend. As κ_D also fixes independently cutoff frequencies via water conductivity, the analysis is clearly consistent. However, it should be kept in mind that despite its remarkable description of the experimental data, the theory of Ref. [14] is for a single bilayer in a symmetric environment, unlike the experimental conditions used here.

The electroformation technique uses similar electric field to destabilize membranes and fabricate Giant Unilamellar Vesicles (GUVs). The stability limit of the bilayers can be calculated using $h(\mathbf{q}) = 0$, and is drawn in Fig. 3.A for two different values of the potential second derivative ($U'' = 3 \times 10^{11}$ J.m^{-4} and 3×10^{12} J.m^{-4}). It clearly shows that our x-rays experiments are performed in the stability

domain but close to instability conditions. With the aim of observing destabilization, we have applied an electric field on a single supported bilayer on an ITO coated glass slide under similar conditions. We observed by fluorescence microscopy the formation of GUVs above and close to the main transition temperature T_m (Fig. 3). Small vesicles of diameter ≈ 5 μm are the dominant population at short times ($t \sim$ 1-10 min) and grow with time to reach a diameter of 10-30 μm. Interestingly, the initial size we find here is consistent with the instability in the bilayer fluctuation spectra evidenced by x-ray scattering.
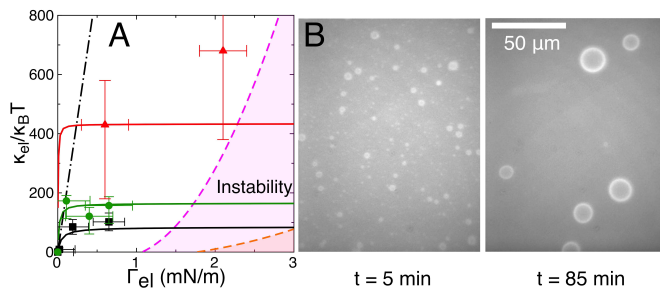

FIG. 3: Γ_{el} as a function of K_{el} (A). The destabilization limits for $U'' = 10^{12.5}$ J.m^{-4} and $10^{11.5}$ J.m^{-4} are given as light and dark pink domains respectively. Vesicle formation under electric field (5 V, 5 Hz) from a single supported bilayer of DPPC (B). Observation by fluorescence microscopy at 5 min (left) and 85 min (right) after the application of the field.

The effect of low AC fields on supported floating bilayers has been determined by x-ray off-specular scattering measurements and carefully analyzed both at the electrokinetic level and at the microscopic level of the bilayer elasticity following [14, 15]. At small lengthscales ≤ 0.5 μm, the electric field induces a strong increase in the bilayer bending rigidity, with a saturation related to the electric double layer thickness, whereas at larger lengthscales ≥ 0.5 μm, we observe a dramatic decrease in the membrane tension, possibly down to negative values. The competition between the stabilizing effect on bending rigidity and destabilizing effect on tension can be tuned to achieve vesicle formation with sizes larger than $2\pi\sqrt{\kappa/\gamma} \sim 1$ μm as observed by optical microscopy, the fastest growing mode being selected by hydrodynamics [13]. This detailed understanding can now be used for further analysis of the effect of electric fields on biological membranes. For cell membranes which have a smaller rigidity ($\sim 1-10\,k_BT$) than our model membrane, destabilization is expected to occur at lengthscales $\simeq 50$ nm and could explain the effect of low electric fields in processes like electroendocytosis.

Acknowledgments

[1] M. Angelova and D. Dimitrov, Faraday Discuss. Chem. Soc. **81**, 303 (1986).
[2] K. A. Riske and R. Dimova, Biophysical Journal **88**, 1143 (2005).
[3] R. Dimova, N. Bezlyepkina, M. Domange Jordo, R. Knorr, K. Riske, M. Staykova, P. Vlahovska, T. Yamamoto, P. Yang, and R. Lipowsky, Soft Matter **5**, 3201 (2009).
[4] P. F. Salipante, M. L. Shapiro, and P. M. Vlahovska, Procedia IUTAM **16**, 60 (2015).
[5] T. Hianik, Reviews in Molecular Biotechnology **74**, 189 (2000).
[6] M. Zhao, B. Song, J. Pu, T. Wada, B. Reid, G. Tai, F. Wang, A. Guo, P. Walczysko, Y. Gu, T. Sasaki, A. Suzuki, J. Forrester, H. Bourne, C. Devreotes, P.N. McCaig, and J. Penninger, Nature **442**, 457 (2006).
[7] U. Zimmermann, in *Reviews of Physiology*, Vol. 105 (Springer Berlin Heidelberg, 1986) pp. 175–256.
[8] U. Zimmermann and G. Neil, *Electromanipulation of cells* (CRC press, 1996).
[9] R. S. Son, K. C. Smith, T. R. Gowrishankar, P. T. Vernier, and J. C. Weaver, J Membr Biol **247**, 1209 (2014).
[10] L. Rems, M. Usaj, M. Kanduser, M. Rebersek, D. Miklavcic, and G. Pucihar, Sci Rep **3**, 3382 (2013).
[11] P. Vernier, Y. Sun, and M. Gundersen, BMC Cell Biology **7**, 37 (2006).
[12] P. M. Vlahovska, Soft Matter **11**, 7232 (2015).
[13] P. Sens and H. Isambert, Physical Review Letters **88**, 128102 (2002).
[14] F. Ziebert and D. Lacoste, New Journal of Physics **12**, 095002 (2010).
[15] F. Ziebert and D. Lacoste, Advances in planar lipid bilayers and liposomes, vol. 14 , 63 (2011).
[16] G. Fadda, D. Lairez, Z. Guennouni, and A. Koutsioubas, Physical Review Letters **111**, 028102 (2013).
[17] see Supplemental Material at [] for more details on modeling.
[18] A. Hemmerle, L. Malaquin, T. Charitat, S. Lecuyer, G. Fragneto, and J. Daillant, Proceedings of the National Academy of Sciences **109**, 19938 (2012).
[19] see Supplemental Material at [] for more details on experimental methods.
[20] L. Malaquin, T. Charitat, and J. Daillant, Eur. Phys. J. E **31**, 285 (2010).
[21] D. Haughey and J. C. Earnshaw, Colloids and Surfaces A: Physicochemical and Engineering Aspects **136**, 217 (1998).
[22] W. M. Haynes, *CRC handbook of chemistry and physics* (CRC press, 2013).
[23] H. I. Petrache, N. Gouliaev, S. Tristram-Nagle, S. Zhang, R. M. Suter, and J. F. Nagle, Physical Review E **57**, 7014 (1998).
[24] K. Mallikarjunaiah, A. Leftin, J. J. Kinnun, M. J. Justice, A. L. Rogozea, H. I. Petrache, and M. F. Brown, Biophysical journal **100**, 98 (2011).

Supplemental Material for
Reduction in Tension and Stiffening of Lipid Membranes in an
Electric Field Revealed by X-ray Scattering

A. Hemmerle, J. Daillant, G. Fragneto, T. Charitat

January 3, 2016

Contents

After introducing the notation we used, we present the main theoretical models used for describing our data in section 2. The first one is an extension of Ziebert and Lacoste's electrokinetic model [1] to our experimental configuration (section 2.1.1). It allows to calculate the electric potential and electric field in the cell in the case of an applied AC electric field, assuming that the membranes are strictly planar and non-fluctuating. In a second step (section 2.2), we present how to calculate the modification of mechanical parameters for a single free bilayer in a static electric field, in the framework of the non-linearized Poisson-Boltzmann theory, following the work of Ziebert and Lacoste [2, 1]. Section 3 is devoted to Material and Methods. We give all the experimental off-specular reflectivity data together with the best fits we have obtained and the corresponding Electron Density Profile (EDP) (section 3.4). All the fitted parameters are summarized in a table in section 3.5. Finally, we give some details on the calculation of number of water molecules in section 4.

1   Notations

- $e = 1.6 \cdot 10^{-19}$ C, elementary charge.
- $k_B = 1.38 \cdot 10^{-23}$ J/K, Boltzmann constant.
- $\epsilon_0 = 8.8541 \cdot 10^{-12}$ F/m, electric permittivity of a vacuum.
- $\epsilon_m = 2\epsilon_0$, electric permittivity of membranes.
- $\epsilon_w = 80\epsilon_0$, electric permittivity of water.
- A, sample surface.
- $\Phi(\mathbf{r}) = \Phi(z)$, electric potential.
- $\mathbf{E}(\mathbf{r}) = E(z)\,\mathbf{u}_z$, electric field.
- $n_-(\mathbf{r}) = n_-(z)$, density of anions.
- $n_+(\mathbf{r}) = n_+(z)$, density of cations.
- D, diffusion coefficient of ionic species.
- $\mathbf{j}(\mathbf{r}) = j(z)\,\mathbf{u}_z$, electric current density.
- V_{loc}, local electric potential at the floating membrane + electric double layers boundaries (Fig. S3).
- Z, total impedance of the system.
- Z_B, bulk impedance.
- Z_m, membrane impedance.
- Z_{DL}, electric double layer impedance.
- Z_{Si}, silicon oxyde impedance.
- $L = 0.5$ cm, experimental cell size.
- d_w, intermembrane water layer thickness.
- d, membrane thickness.
- d_{Si}, silicon oxyde layer thickness.
- Γ_{el} electric correction to the membrane tension.
- K_{el} electric correction to the membrane bending rigidity.

2 Modeling

2.1 Electrokinetic modeling

2.1.1 Generalization of Ziebert and Lacoste model

The model Ziebert and Lacoste [2] consider a single bilayer in a symmetric environment. Extending their model [1] for our experimental configuration, we calculate here the electric potential and electric field in the cell in the case of an applied AC field for planar, non-fluctuating membranes.
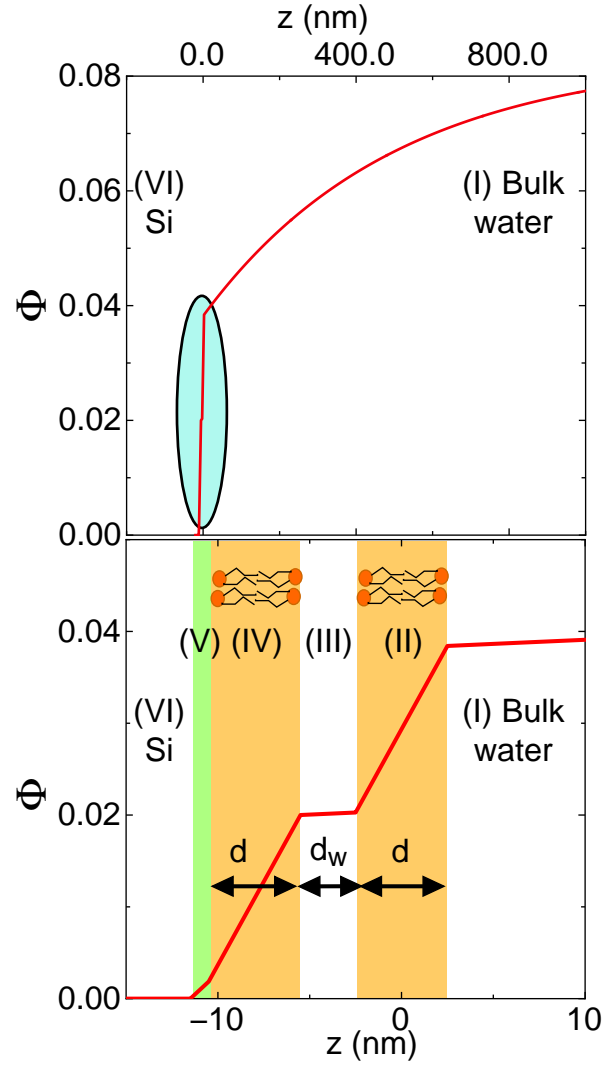

Figure S1: Electrostatic potential Φ as a function of z (top). Zoom on the double bilayer region and definition of the different domains in the system (bottom).

We have the following domains (see Fig. S1):

- **domain I:** bulk water (first electrode) between $z = d/2$ and $z = L$, modeled as an electrolyte of Debye length κ_D^{-1} and permittivity ϵ_w;

- **domain II:** a floating bilayer of thickness d centered in $z = 0$, modeled as an insulator of permittivity ϵ_m;

- **domain III:** an interbilayer water layer of thickness d_w between $z = -d/2$ and $z = -d/2 - d_w$, modeled as an electrolyte of Debye length κ_D^{-1} and permittivity ϵ_w;

- **domain IV:** a supported bilayer of thickness d between $z = -d/2 - d_w$ and $z = -d/2 - d_w - d$, modeled as an insulator of permittivity ϵ_m;

- **domain V:** a silicon oxide layer of thickness d_{Si} between $z = -3d/2 - d_w$ and $z = -3d/2 - d_w - d_{Si}$, modeled as an insulator of permittivity ϵ_{Si};

The silicon block at $z = -3d/2 - d_w - d_{Si}$ is grounded ($\Phi = 0$) and the counterelectrode at $z = L$ is at potential $\Phi = V$.

In the electrolyte, we have to solve the Poisson-Nernst-Planck equations:

$$\epsilon_w \partial_z^2 \Phi = -e(n_+ - n_-), \tag{1}$$

$$e\partial_t n^\pm = -\partial_z j^\pm, \tag{2}$$

$$j^\pm = -D\left(e\partial_z n^\pm \mp n^\pm \frac{e^2}{k_B T} \partial_z \Phi\right). \tag{3}$$

In insulating domains, we have to solve the Poisson equation:

$$\partial_z^2 \Phi = 0, \tag{4}$$

with continuity relations at each interface.

In the following we note:

$$\beta(\omega, \kappa_D, I_0, D) = \kappa_D \sqrt{1 + \frac{j\omega}{D\kappa_D^2}}, \tag{5}$$

$$\lambda_m = \frac{\epsilon_w}{\epsilon_m} d. \tag{6}$$

Charge density and electrostatic potential In domain I (bulk) the charge density $\rho^{(I)}$ and the potential $\Phi^{(I)}$ are given by:

$$\rho^{(I)}(z, V, L, \kappa_D, I_0, D, \omega) = \frac{j\kappa_D^2 I_0 \sinh(\beta(z-L))}{\omega\beta\cosh(\beta L)}, \tag{7}$$

$$\Phi^{(I)}(z, V, L, \kappa_D, I_0, D, \omega) = V + \frac{(I_0(z-L) - D\rho^{(I)})}{\epsilon_w D\beta^2}. \tag{8}$$

In domain II (bilayer), the charge density is 0 and the potential is a linear function. By writing the continuity of the potential and the electric field we can write:

$$\rho^{(II)}(z, V, L, \kappa_D, I_0, D, \omega) = 0, \tag{9}$$

$$\Phi^{(II)}(z, V, L, \kappa_D, I_0, D, \omega) = \Phi^{(I)}(d/2, V, L, \kappa_D, I_0, D, \omega) + \frac{I_0\left(z - \frac{d}{2}\right)}{j\omega\epsilon_m}. \tag{10}$$

By using the same approach it is possible to write the charge density and the potential in domain III. Integrating Poisson equation Eq. 4, we have:

$$\rho^{(III)}(z, V, L, \kappa_D, I_0, D, \omega) = \frac{jI_0\kappa_D^2}{\beta\omega} \frac{\left(e^{\beta d_w}e^{\beta(z+d/2)} - e^{-\beta(z+d/2)}\right)}{1 + e^{\beta d_w}}, \tag{11}$$

$$\Phi^{(III)}(z, V, L, \kappa_D, I_0, D, \omega) = c_2 + \frac{I_0 z - D\rho^{(III)}}{D\beta^2\epsilon_w}, \tag{12}$$

S4

with c_2 an integration constant which is fixed by ensuring the water layer electroneutrality :

$$\int_{-d/2}^{-d/2-d_w} \rho^{(III)}(z)\, dz = 0.$$

In domain IV we have:

$$\rho^{(IV)}(z, V, L, \kappa_D, I_0, D, \omega) = 0, \tag{13}$$

$$\Phi^{(IV)}(z, V, L, \kappa_D, I_0, D, \omega) = \Phi^{(III)}(-(d_w + d/2))$$

$$+ \quad \frac{I_0 \left(1 - \jmath D\kappa_D^2\right)}{D\beta^2 \epsilon_m}\left(z + \frac{d}{2} + d_w\right). \tag{14}$$

In domain V:

$$\rho^{(V)}(z, V, L, \kappa_D, I_0, D, \omega) = 0, \tag{15}$$

$$\Phi^{(V)}(z, V, L, \kappa_D, I_0, D, \omega) = \Phi^{(IV)}\left(-\left(d_w + \frac{3}{2}d\right)\right)$$

$$+ \quad \frac{I_0 \left(1 - \jmath D\kappa_D^2\right)}{D\beta^2 \epsilon_{Si}}\left(z + \frac{3}{2}d + d_w\right). \tag{16}$$

Impedance We then impose that the potential vanishes on the silicon electrode:

$$\Phi^{(V)}\left(-(\frac{3}{2}d + d_w + d_{Si})\right) = 0,$$

leading to a linear relation between I_0 and V that allows us to define the system impedance:

$$Z(\omega, \kappa_D)\, A = \left[\frac{\beta}{D}\left\{\epsilon_{Si}\left(2\epsilon_w - \epsilon_m\right)d + 2\epsilon_m\left(\epsilon_w d_{Si} + \epsilon_{Si}\left(d_w + L\right)\right)\right\}\right.$$

$$+ \quad \frac{2}{\jmath\omega}\left\{\left(\epsilon_{Si}d + \epsilon_m d_{Si}\right)\epsilon_w\beta\kappa_D^2 + \epsilon_{Si}\epsilon_w d\beta^3\right.$$

$$+ \quad \left.\left.\epsilon_{Si}\epsilon_m\kappa_D^2\left(\frac{\sinh\left(\beta\left(L - d/2\right)\right)}{\cosh\left(\beta L\right)} + 2\tanh\left(\frac{\beta d_w}{2}\right)\right)\right\}\right] / \left(2\epsilon_{Si}\epsilon_m\epsilon_w\beta^3\right). \tag{17}$$

The potential is represented on figure S1 for $\kappa_D^{-1} = 500$ nm and $f = 10$ Hz.

It is then possible to rearrange Eq. 17:

$$Z(\omega, \kappa_D) \quad = \quad Z_{Si}(\omega) + Z_B(\omega, \kappa_D) + Z_{DL}(\omega, \kappa_D)$$

$$+ Z_{S,1}(\omega, \kappa_D) + Z_{S,2}(\omega, \kappa_D), \tag{18}$$

schematically represented in Fig. S2, where

$$Z_{SiO_2}(\omega) = \frac{d_{Si}}{\jmath\omega\epsilon_{Si}A}, \tag{19}$$

is the SiO_2 impedance (purely capacitive),

$$Z_{S,1}(\omega) = \frac{d}{\jmath\omega\epsilon_m A}, \tag{20}$$

is the supported bilayer impedance (purely capacitive),

$$Z_{S,2}(\omega, \kappa_D) = \frac{d}{AD\epsilon_m\beta^2} = \frac{1}{R_m^{-1} + \jmath\omega C_m}, \tag{21}$$

S5

is the floating bilayer impedance (capacitance $C_m = \epsilon_m A/d$ and resistance $R_m = d/(D\kappa_D^2 \epsilon_m A)$ in parallel), and

$$Z_B(\omega, \kappa_D) = \frac{(L + d_w - d/2)}{AD\epsilon_w \beta^2} = \frac{1}{R_B^{-1} + \jmath\omega C_B}, \tag{22}$$

is the bulk impedance (capacitance $C_B = \epsilon_w A/(L + d_w - d/2)$ and resistance $R_B = (L + d_w - d/2)/(D\kappa_D^2 \epsilon_w A)$ in parallel).

Finally Z_{DL} is the impedance attributed to the two electric double layers:

$$Z_{DL}(\omega, \kappa_D) = \frac{1}{\jmath\omega} \frac{\kappa_D^2}{D\epsilon_w \beta^2} \left[\frac{\sinh(\beta(L - d/2))}{\cosh(\beta L)} + 2\tanh\left(\frac{\beta d_w}{2}\right) \right]. \tag{23}$$

When $L \gg \kappa_D^{-1} \gg d_w$ we obtain:

$$Z_{DL}(\omega, \kappa_D) \simeq \frac{1}{\jmath\omega C_{DL}}, \tag{24}$$

with $C_{DL} = \epsilon_w A/(\kappa_D^{-1} + d_w + \lambda_m)$. The Debye layers behave as a capacitance.
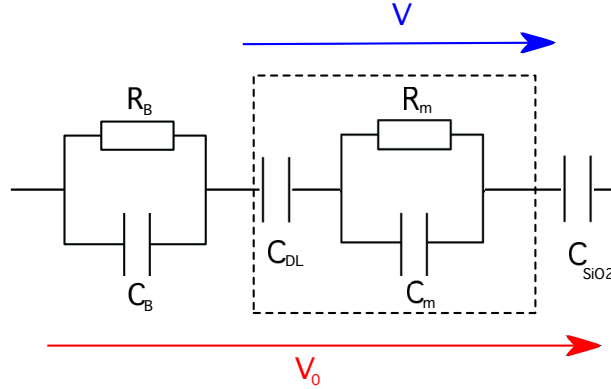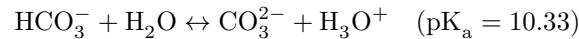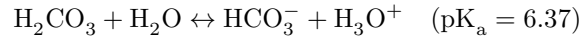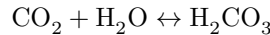

Figure S2: Schematic representation of equivalent circuit for the experimental set-up.

We are thus in the configuration of Fig.S2 with an additional capacitance for the supporting bilayer.

Orders of magnitude The bulk solution resistivity $\rho_s(\kappa_D^{-1})$ depends on the Debye length κ_D^{-1}. Due to the dissolution of CO_2 in water, Debye length decreases from 960 nm for pure water to $\sim 100 - 200$ nm and pH from 7 to 5.8. Dissociation of CO_2 in water leads to various species following the reactions:

$$CO_2 + H_2O \leftrightarrow H_2CO_3$$

$$H_2CO_3 + H_2O \leftrightarrow HCO_3^- + H_3O^+ \quad (pK_a = 6.37)$$

$$HCO_3^- + H_2O \leftrightarrow CO_3^{2-} + H_3O^+ \quad (pK_a = 10.33)$$

At pH$\sim 5 - 6$, the dominant forms are HCO_3^- and H_3O^+. The diffusion coefficients of HCO_3^- and H_3O^+ are $1.18 \cdot 10^{-9}$ m^2.s^{-1} and $7.15 \cdot 10^{-9}$ m^2.s^{-1} [3] respectively. The curves presented in the paper are calculated with a single ion diffusion coefficient D which is taken to be $7.15 \cdot 10^{-9}$ m^2.s^{-1}, as H_3O^+ has the highest mobility. Using these values we find:

- a resistance ranging from 0.5 MΩ.cm^2 to 10 MΩ.cm^2;

- a characteristic time for the bulk is $C_B R_B \sim 5\mu$s, meaning that the capacitive behavior of the bulk is negligible in the working frequency range;

- a bilayer resistance ranging from 20 Ω.cm^2 ($\kappa_D^{-1} = 150$ nm) to 300 Ω.cm^2 ($\kappa_D^{-1} = 800$ nm);

- the silicon oxide capacitance is given by $C_{SiO_2} = \epsilon_{SiO_2}/d_{SiO_2} \sim 4 \cdot 10^9 \epsilon_0$;

- the membrane capacitance is given by $C_m = \epsilon_m/d \sim 4 \cdot 10^8 \epsilon_0$;

- the Debye layer capacitance is given by $C_{DL} = \epsilon_w/(d_w + \epsilon_w/\epsilon_m d + \kappa_D^{-1}) \sim 0.5 - 2 \cdot 10^8 \epsilon_0$;

We then obtain:

$$C_m \sim C_{DL} \ll C_{SiO_2} \quad \text{and} \quad R_m \ll R_B. \tag{25}$$

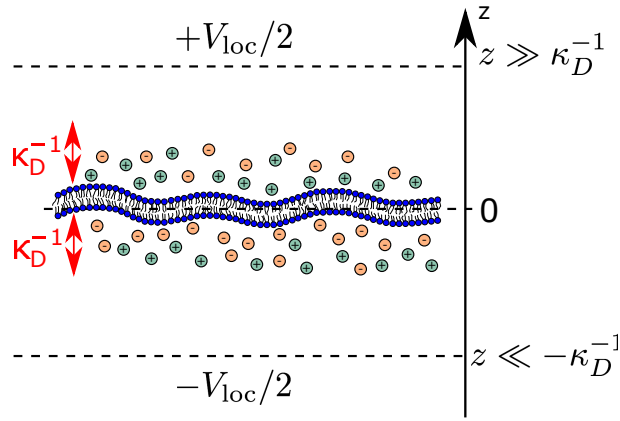### 2.1.2 Electric field at floating bilayer level

Figure S3: Schematic representation of the floating bilayer cell: a quasi-planar bilayer is embedded in a symmetric electrolyte of Debye length κ_D^{-1} and a voltage difference V_{loc} is applied far from the membrane $z \gg \kappa_D^{-1}$.

Calculating the effect of the electric field on the floating bilayer (see Section 2.1.2) implies a precise knowledge of the electric field and electric double layer structure around the bilayer. The solution of the full non-linearized Poisson-Boltzmann equation considering only the floating bilayer is given below, following Ziebert and Lacoste [2]. We consider a neutral and insulating bilayer of thickness d in a monovalent electrolyte characterized by its Debye length κ_D^{-1} only and submitted to a steady voltage V_{loc} ($-V_{loc}/2$ and $V_{loc}/2$ far away from the membrane ($z \gg \kappa_D^{-1}$), see Fig. S3). We first give the local potential V_{loc} using the previously described electrokinetic model.

Local electrostatic potential V_{loc} In order to calculate the local tension V_{loc} acting on the floating bilayer and the electric double layers, we use the results of section 2.1.1:

$$V_{\text{loc}}(\omega, V_0) = \left| \frac{Z_m}{Z} \right| V_0, \tag{26}$$

where

$$Z_m(\omega, \kappa_D) = Z_{S,2}(\omega, \kappa_D) + Z_{DL}(\omega, \kappa_D,), \tag{27}$$

$$Z(\omega, \kappa_D) = Z_B(\omega, \kappa_D) + Z_{DL}(\omega, \kappa_D) + Z_{S,1}(\omega) + Z_{S,2}(\omega, \kappa_D) + Z_{SiO_2}(\omega, \kappa_D). \tag{28}$$

Using Eq. 25 it can be simplified as:

$$V_{\text{loc}} = \sqrt{\frac{1 + (\omega\tau_1)^2}{1 + (\omega\tau_2)^2 + (\omega\tau_3)^4}} V_0, \tag{29}$$

with

$$\tau_1 = R_m(C_m + C_{DL}), \tag{30}$$

$$\tau_2 = \sqrt{R_B^2 C_{DL}^2 + R_m^2(C_m^2 + C_m C_{DL})}, \tag{31}$$

$$\tau_3 = \sqrt{R_m R_B C_m C_{DL}}, \tag{32}$$

and $\tau_1 \ll \tau_3 \ll \tau_2$.

We have a low-pass filter with a cut-off frequency f_c which is a solution of:

$$(\omega\tau_3)^4 + ((\tau_2^2 - \tau_1^2)\omega)^2 - 1 = 0, \tag{33}$$

leading to

$$2\pi f_c = \frac{1}{\sqrt{2}} \frac{\tau_0}{\tau_3^2} \sqrt{\sqrt{1 + 4\left(\frac{\tau_3}{\tau_0}\right)^4} - 1}, \tag{34}$$

where we have used $\tau_0 = \sqrt{\tau_2^2 - \tau_1^2}$.

In our case $\tau_1 \ll \tau_3 \ll \tau_2$ and we have simply:

$$\tau_0 \sim \tau_2 \tag{35}$$

$$2\pi f_c \sim \frac{1}{\tau_2}. \tag{36}$$

Using conditions 25 we have $\tau_2 \sim R_B C_{DL}$ and we obtain the cut-off frequency :

- for $\kappa_D^{-1} \sim 150$ nm, $f_c \simeq 2 - 3$ Hz;

- for $\kappa_D^{-1} \sim 800$ nm, $f_c \simeq 0.2$ Hz.

Self-consistent equation for local electric field   Solving the Poisson-Boltzmann equation leads to the following relation for the local electric field acting on the membranes:

$$E_m(V_{\text{loc}}, \kappa_D) = \frac{4k_B T}{ed}\left(\log\left\{\frac{1+c}{1-c}\right\} - \frac{eV_{\text{loc}}}{k_B T}\right) \tag{37}$$

where $c(V_{\text{loc}}, T, \kappa_D, d) \in (0, 1)$ is given by the self-consistent equation:

$$\frac{\epsilon_m}{\epsilon_w}\left(\frac{eV_{\text{loc}}}{k_B T} - 4\log\left\{\frac{1+c}{1-c}\right\}\right) = 4\kappa_D d\left(\frac{c}{1-c^2}\right). \tag{38}$$

Numerical solutions of this self-consistent equation are presented in Fig. S4 for various conditions. The linear low voltage limit is in agreement with the calculations based on the Debye-Hückel approximation of [4] (dotted-dashed line). Finally, we report on Fig. S4 (right) the values corresponding of our experimental conditions clearly showing that we experimentally access the non-linear regime.
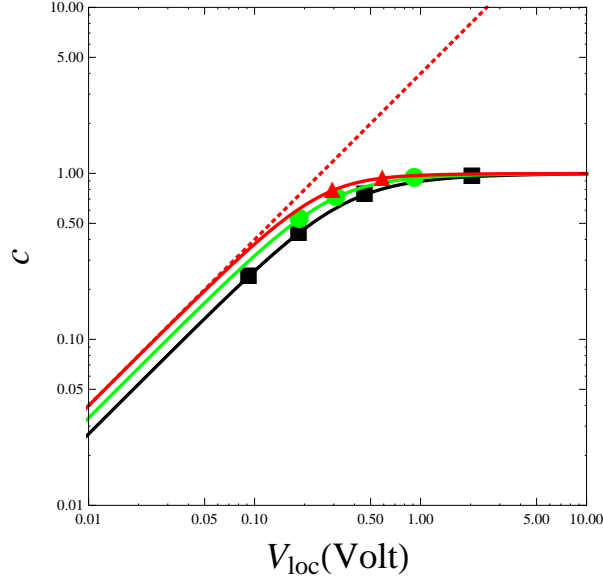
S8

Figure S4: Solid line: numerical solution of Eq. 38 for $c\left(V_{\mathrm{loc}}, T, \kappa_D, d\right)$ as a function of V_{loc} for $\kappa_D^{-1} = 150$ (black), 300 (green) and 800 nm (red). Dashed-dotted red line: linear Debye-Hückel solution for $\kappa_D^{-1} = 150$ nm. Solid symbols correspond to our experimental conditions.

2.2 Floating bilayer mechanical properties in an electric field

Again following Ziebert and Lacoste [2, 1], we use the solution of the non-linearized Poisson-Boltzmann equation (see section 2.1.2) to determine the effect of the electric field on the bilayer. We still consider a single neutral and insulating floating bilayer of thickness d, surface tension γ and bending modulus κ in a monovalent electrolyte characterized by its Debye length κ_D^{-1}. The membrane is fluctuating and supposed to be flat enough to be described within the Monge representation by a height function $h(r_\perp)$, where $r_\perp$ is a two-dimensional in-plane vector. The potential is assumed to be equal to $-V_{loc}/2$ and $V_{loc}/2$ far away from the membrane ($z \gg \kappa_D^{-1}$).

Knowing the electric field (see section 2.1.2) and solving in Stokes approximation the hydrodynamics problem of the electrolyte around the membrane, Ziebert and Lacoste calculate the total stress tensor as :

$$\tau_{ij} = -p\delta_{ij} + \eta\left(\partial_i v_j + \partial_j v_i\right) + \epsilon\left(E_i E_j - \frac{1}{2}\delta_{ij}E^2\right). \tag{39}$$

Ensuring the force balance equation supposes to compensate the discontinuity of the normal/normal component of the stress tensor and the restoring force due to membrane elasticity, leading to the an expression of membrane fluctuation's growth rate. Performing an expansion with respect to the membrane height field, one obtains at zero order the electrostatic pressure acting on the flat membrane, and at order one the contribution of the electric field to both the surface tension and the bending modulus (for details see [2, 1]).

2.2.1 Electrostatic pressure

Using the previous description at zero order, the electric field exerts an electrostatic pressure on the bilayer that can be calculated as:

$$\Pi_{el} = \int_{d/2}^{L} dz \rho^{(I)}(z) E^{(I)}(z) - \int_{-d/2-d_w}^{d_w} dz \rho^{(III)}(z) E^{(III)}(z)$$

$$= \epsilon_w \int_{d/2}^{L} dz E^{(I)}(z) \frac{dE^{(I)}(z)}{dz} - \epsilon_w \int_{-d/2-d_w}^{d_w} dz E^{(III)}(z) \frac{dE^{(III)}(z)}{dz}$$

$$= \frac{1}{2} \epsilon_w \left(E^{(I)}(z)^2 \right)_{d/2}^{L} - \frac{1}{2} \epsilon_w \left(E^{(III)}(z)^2 \right)_{-d/2-d_w}^{d_w}. \tag{40}$$

Using the expressions of the electrostatic potential in each domain it is possible to obtain the electric field. We obtain:

$$\Pi_{el} = \frac{1}{2} \frac{I_0^2}{D^2 \epsilon_w \beta^4} \left(\left(1 - \jmath \frac{D\kappa_D^2}{\omega} \frac{1}{\cosh(\beta L)} \right)^2 - \left(1 - \jmath \frac{D\kappa^2}{\omega} \frac{\cosh(\beta(L-d/2))}{\cosh(\beta L)} \right)^2 \right).$$

In the next section we analyze our experimental results combining these two models. It should be noticed that we have essentially only one unknown parameter which is the Debye length of the solution. All other parameters are well known from the literature and the experimental conditions.

2.2.2 Surface tension

The electrostatic correction to the surface tension Γ_{el} has a contribution due to the electric field inside the membrane Γ_m and another one due to the electric double layers Γ_{DL}:

$$\Gamma_{el}(V_{\rm loc}, \kappa_D) = \Gamma_m(V_{\rm loc}, \kappa_D) + \Gamma_{DL}(V_{\rm loc}, \kappa_D). \tag{41}$$
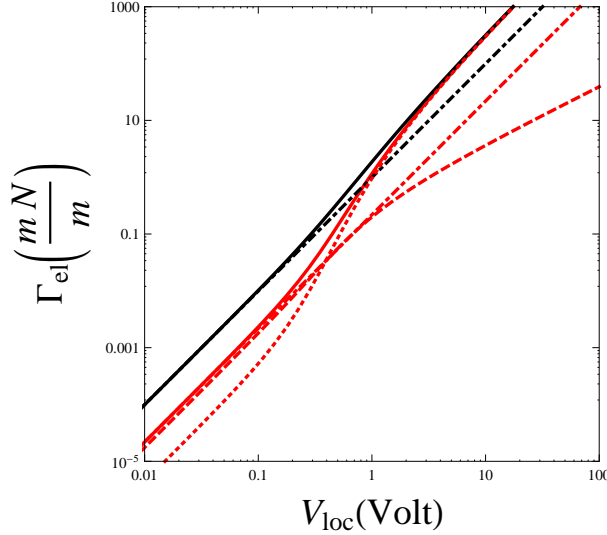

Figure S5: Γ_{el} for $\kappa_D^{-1} = 150$ nm (black solid line) and $\kappa_D^{-1} = 800$ nm (red solid line) and corresponding linear Debye-Hückel solutions (dotted-dashed line). Membrane (Γ_m, dotted line) and Debye layers (Γ_{DL}, dashed line) contributions are also shown for $\kappa_D^{-1} = 800$ nm.

Using the solution of the Poisson-Boltzmann (PB) equation for the electric field, Ziebert and Lacoste [2] obtain:

$$\Gamma_m\left(V_{\text{loc}}, \kappa_D\right) \;=\; -\epsilon_m d E_m^2, \tag{42}$$

$$\Gamma_{DL}\left(V_{\text{loc}}, \kappa_D\right) \;=\; -16\epsilon_w\kappa_D\left(\frac{eV_{\text{loc}}}{k_BT}\right)^2 \frac{c^2}{1-c^2}. \tag{43}$$

It is possible to express asymptotic expressions for Γ_{DL}:

$$\text{for } \frac{eV_{\text{loc}}}{k_BT} \gg 1, \quad \Gamma_{DL}\left(V_{\text{loc}}, \kappa_D\right) \simeq -4\epsilon_m \frac{k_BT}{e} \frac{V_{\text{loc}}}{d} \tag{44}$$

$$\text{for } \frac{eV_{\text{loc}}}{k_BT} \ll 1, \quad \Gamma_{DL}\left(V_{\text{loc}}, \kappa_D\right) = -\frac{\epsilon_m^2}{\epsilon_w} \frac{\kappa_D V_{\text{loc}}^2}{(2\frac{\epsilon_m}{\epsilon_w} + \kappa_D d)^2}. \tag{45}$$

Fig. S5 left-hand side shows the comparaison between the exact numerical solution for Γ_{DL} with the asymptotic expressions. On right hand-side, the total electrostatic surface tension Γ_{el} and the both membrane Γ_m and Debye layer Γ_{DL} contributions are represented for two Debye lengths. We clearly observe that for voltage $\gg 0.1$ V the membrane gives the main contribution. In this regime we also observe a clear deviation to the linear Debye-Hückel approximation (dotted-dashed line).

2.2.3 Bending modulus

As for the surface tension, the electrostatic corrections to the bending modulus K_{el} has a contribution due to the electric field inside the membrane K_m and another one due to the electric double layers K_{DL}:

$$K_{el}\left(V_{\text{loc}}, \kappa_D\right) \;=\; K_m\left(V_{\text{loc}}, \kappa_D\right) + K_{DL}\left(V_{\text{loc}}, \kappa_D\right). \tag{46}$$
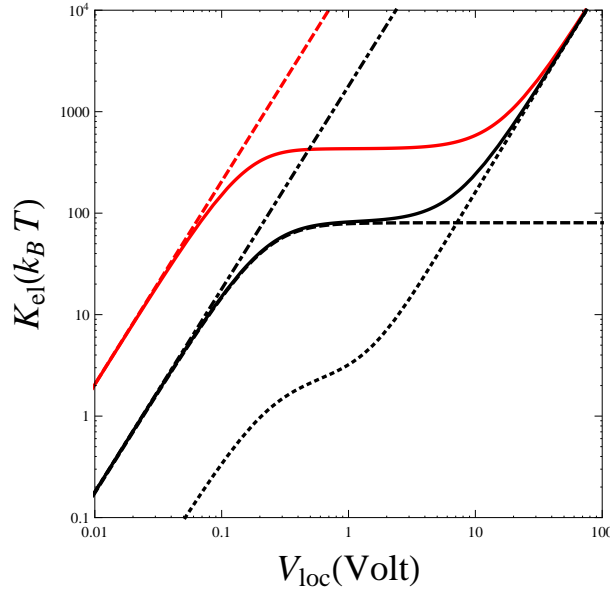

Figure S6: K_{el} for $\kappa_D^{-1} = 800$ nm (red solid line) and $\kappa_D^{-1} = 150$ nm (black solid line) and linear (Debye-Hückel) solution (dotted-dashed line). Membrane (K_m, dotted line) and Debye layers (K_{DL}, dashed line) contributions are also shown for $\kappa_D^{-1} = 150$ nm.

Again, using the PB solution for the electric field, Ziebert and Lacoste [2] obtain:

$$K_{DL}\left(V_{\text{loc}}, \kappa_D\right) = \frac{4\epsilon_w}{\kappa_D}\left(\frac{k_BT}{e}\right)^2\left(\frac{3-c^2}{1+c^2}\right)c^2, \tag{47}$$

$$K_m\left(V_{\text{loc}}, \kappa_D\right) = \epsilon_m E_m^2\left(\frac{d^3}{12} - \frac{2k_BT\kappa_D^{-1}d}{eE_m}\left(\frac{1-c^2}{1+c^2}\right)c\right). $$

Again it is possible to obtain the following asymptotic expressions for K_{DL}:

$$\text{for } \frac{eV_{\text{loc}}}{k_BT} \gg 1, \quad K_{DL}\left(V_{\text{loc}}, T, \kappa_D, d\right) = 4\epsilon_w\kappa_D^{-1}V_{\text{loc}}^2, \tag{48}$$

$$\text{for } \frac{eV_{\text{loc}}}{k_BT} \ll 1, \quad K_{DL}\left(V_{\text{loc}}, T, \kappa_D, d\right) = \frac{3}{4}\epsilon_w\frac{V_{\text{loc}}^2}{\left(2\kappa_D^{-1} + \lambda_m\left(d\right)\right)^2}. \tag{49}$$

Fig. S6 left-hand side shows the comparaison between the exact numerical solution for K_{DL} with the asymptotic expressions. On right hand-side, the total electrostatic bending modulus K_{el} and both membrane K_m and Debye layer K_{DL} contributions are represented for two Debye lengths. For voltage lower than 10 V the membrane contribution is negligible. The Debye layer present a saturation plateau which value is directly related to κ_D^{-1}.

3   Experimental datas and analysis

3.1   Samples preparation

DSPC ($L-\alpha$ 1,2-distearoyl-sn-glycero-3-phosphocholine, Avanti Polar Lipids, Lancaster, Alabama) supported bilayers were prepared by depositing two bilayers on ultra-flat silicon substrates (SESO, France) using a Langmuir trough filled with ultra pure water (18.2 MΩ.cm) from a Millipore purification system. First three monolayers were deposited using the classical Langmuir-Blodgett method and the last one using Langmuir-Schaefer deposition (horizontal sample) [5]. The first bilayer serves as a spacer to reduce the interaction between the floating bilayer and the substrate and keeps it free to fluctuate. Samples were inserted into a PTFE sample cell with 50 μm thick windows embedded in an Al box, and gradually heated in the fluid phase, with a feedback on the cell temperature measured using a Pt100 sensor. Potential was applied between a Cu layer deposited at the back of the thick Si substrate and an ITO coated glass plate mounted parallel to the subtrate in the solution, 0.5 cm from the membrane.

3.2   Off-specular reflectivity

Off-specular reflectivity curves were recorded using the procedure of Ref. [6]. The experiments reported here used a 27 keV x-ray beam (wavelength $\lambda = 0.0459$ nm) at the CRG-IF beamline of the European Synchrotron Radiation Facility (ESRF). The scattering geometry is described in Fig. 1A (main paper). Off-specular reflectivity was recorded at a fixed grazing angle of incidence $\theta_{in} = 0.7$ mrad below the critical angle of total external reflection at the Si-water interface (0.83 mrad) in order to facilitate background subtraction. With this geometry, both q_x and q_z are varied during a scan.

3.3   Data analysis

Off-specular reflectivity is sensitive to both static deformation and thermal fluctuations of a membrane. The linear response theory of Ref. [7] was extended to double bilayers in order to describe the static coupling of the bilayers to the substrate [8] and the thermal correlation functions were derived applying equipartition of energy using a Hamiltonian taking into account the bilayers tensions γ, bending rigidities

κ and interaction potentials via their second derivative [8, 9]. In the simple case of a single bilayer, we have $\mathcal{H} = \int d^2 \mathbf{q} \mathcal{H}(\mathbf{q})$, with $\mathcal{H}(\mathbf{q}) = U'' + \gamma q^2 + \kappa q^4$, leading to a fluctuation spectrum $\langle z(\mathbf{q})z(-\mathbf{q}) \rangle = k_B T / \mathcal{H}(\mathbf{q})$. In the limit of small amplitudes, the scattered intensity is $I_{sc} \propto \langle z(\mathbf{q})z(-\mathbf{q}) \rangle$. Fitting of the scattering curves following the procedure of Refs. [8, 9] therefore gives access to the bilayer electron density profile, γ, κ and interaction potentials. Different scattering curves are presented on Fig. S7, showing that high voltage differences, up to 10 V can be applied to the membrane without destroying it, but strongly affecting its fluctuations.

3.4 Experimental curves

The off-specular reflectivity curves and the associated best fits are presented on figure S7. The Electron Density profile corresponding to the best fit are presented on Fig. S8.
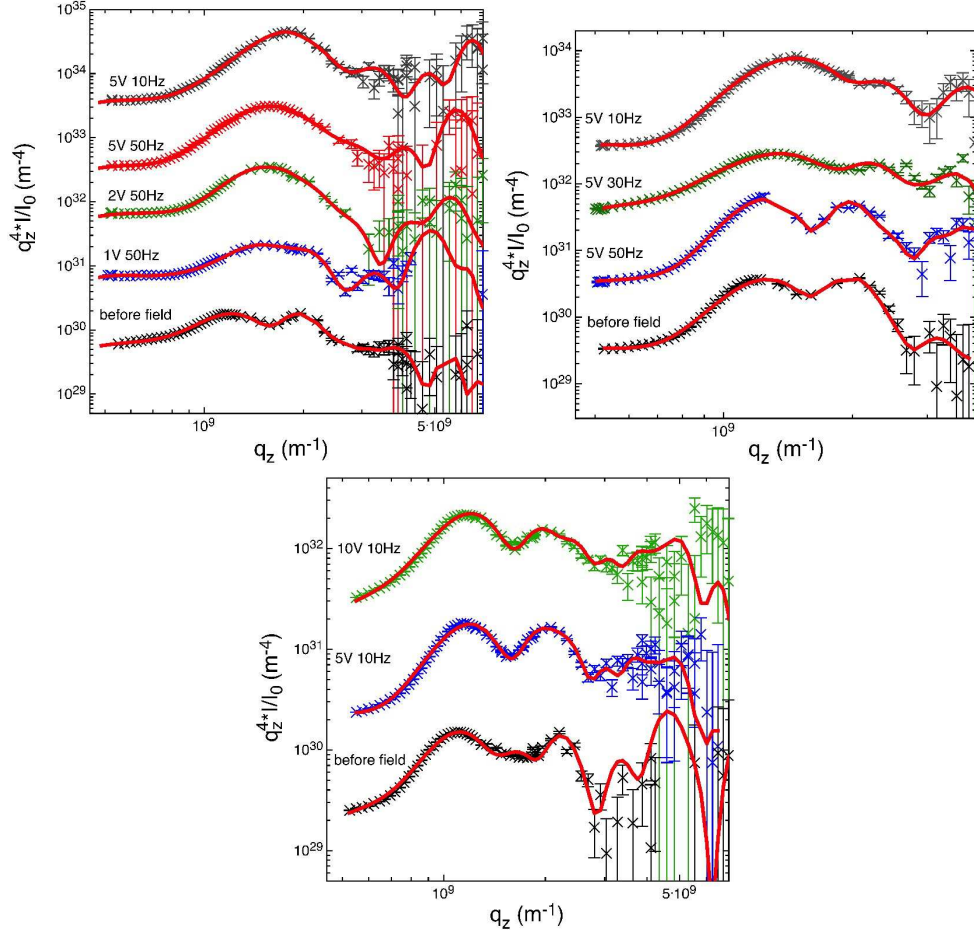

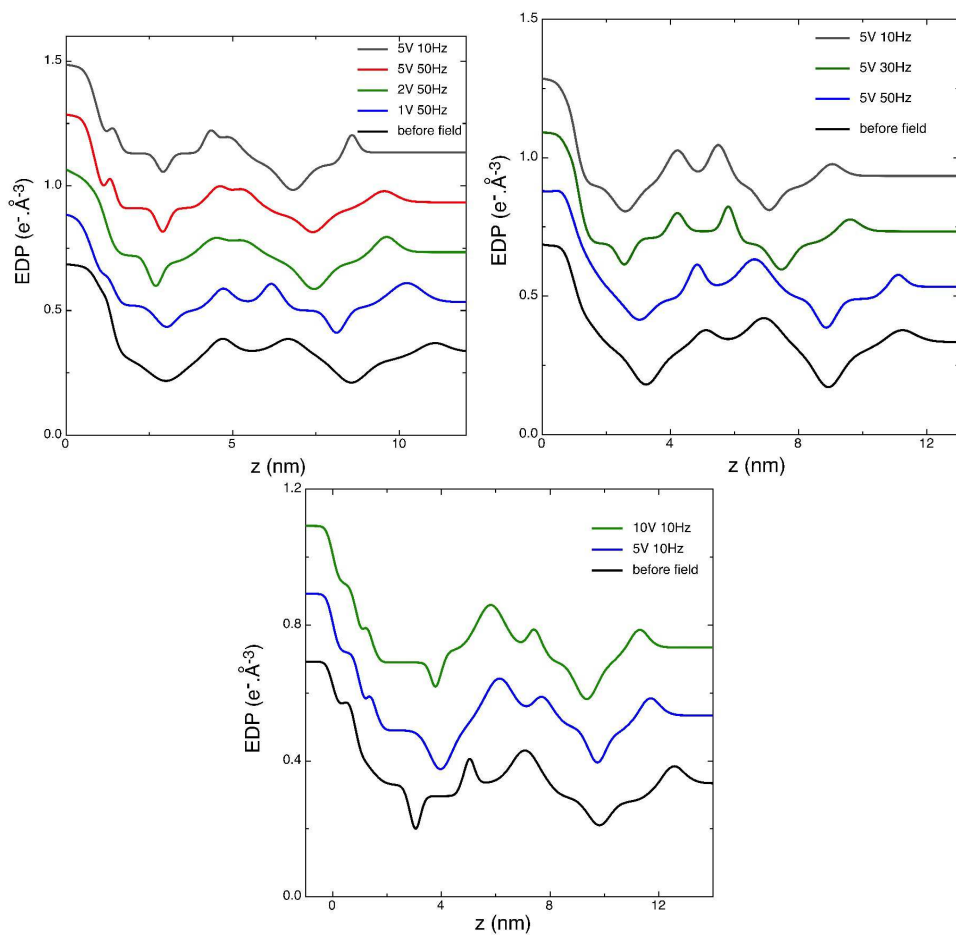Figure S7: Diffuse scattering and best fit (full line).

Figure S8: Electron Density profile corresponding to the best fit of Fig. S7.

3.5 Fitted parameters

Parameters obtained from the best fits presented in Fig. S7 are given in Table S1.

Series 1 (■)	Before field	1 V 50 Hz	2 V 50 Hz	5 V 50 Hz	5 V 10 Hz
d_w[Å]	23.4 ± 1	16.3 ± 1	12.8 ± 1	10.1 ± 1	7.0 ± 1
κ_2 [k_BT]	14 (10-25)	23 (15-35)	81 (60-110)	99 (85-130)	116 (95-130)
γ_2 [mN/m]	0.87 ± 0.2	0.85 ± 0.2	1.08 ± 0.2	0.68 ± 0.2	0.22 ± 0.2
$\sigma_{2,th}$ [Å]	8 ± 0.5	9 ± 1	9 ± 1	10 ± 1	10 ± 1
U''_{M_1,M_2} [10^x J/m^4]	12.96 ± 0.2	12.26 ± 0.2	11.71 ± 0.2	11.43 ± 0.2	11.63 ± 0.2
K_{el} [k_BT]	0	9 (5-10)	67 (50-85)	85 (75-105)	102 (85-105)
Γ_{el} [mN/m]	0	0.02 ± 0.4	-0.21 ± 0.4	0.19 ± 0.4	0.65 ± 0.3
n_w	23.0 ± 2	15.2 ± 2	11.9 ± 2	9.5 ± 2	6.7 ± 2

Series 2 (●)	Before field	5 V 50 Hz	5 V 30 Hz	5 V 10 Hz
d_w[Å]	22.0 ± 1	20.1 ± 1	17.0 ± 1	14.1 ± 1
κ_2 [k_BT]	20 (15-30)	193 (130-250)	141 (120-220)	177 (150-280)
γ_2 [mN/m]	0.78 ± 0.2	0.67 ± 0.2	0.38 ± 0.2	0.13 ± 0.2
$\sigma_{2,th}$ [Å]	9 ± 1.8	8 ± 1	8 ± 1	12 ± 1.7
U''_{M_1,M_2} [10^x J/m^4]	12.9 ± 0.2	12.7 ± 0.2	11.8 ± 0.2	11.0 ± 0.2
K_{el} [k_BT]	0	173 (110-191)	121 (130-201)	157 (180-261)
Γ_{el} [mN/m]	0	0.11 ± 0.3	0.4 ± 0.3	0.65 ± 0.3
n_w	23.2 ± 2	18.8 ± 2	17.6 ± 2	16.4 ± 2

Series 3 (▲)	Before field	5 V 10 Hz	10 V 10 Hz
d_w[Å]	22.5 ± 1	18.4 ± 1	17.3 ± 1
κ_2 [k_BT]	20 (15-40)	450 (200-600)	700 (500-1000)
γ_2 [mN/m]	0.50 ± 0.2	-0.1 ± 0.2	-1.6 ± 0.2
$\sigma_{2,th}$ [Å]	9 ± 2	5 ± 1	6 ± 1.5
U''_{M_1,M_2} [10^x J/m^4]	12.7 ± 0.2	12.9 ± 0.2	12.7 ± 0.2
K_{el} [k_BT]	0	430 (180-581)	680 (480-981)
Γ_{el} [mN/m]	0	0.6 ± 0.3	2.1 ± 0.3
n_w	16.3 ± 2	18.8 ± 2	18.4 ± 2

Table S1: Structural and elastic parameters obtained from the best fits of off-specular data (see Fig. S7).

4 Hydration of the floating bilayer

An important quantity characterizing the hydration of the bilayers is the number of water molecules per lipid n_w located between the two membranes. n_w can be obtained as follows [10]:

$$n_w = \frac{A_L d_w}{2V_w} \tag{50}$$

where $V_w = 30$ Å^3 is the volume of one molecule of water and A_L the area per lipid of the floating bilayer. A_L is calculated by integration of the electron density profile over the fatty acid chains of each monolayer:

$$A_L \int_{ch} \rho(z)dz = 2n_{ch}^*, \tag{51}$$

with n_{ch}^* the number of electron per chain ($n_{ch}^* = 274$ for DSPC).

In Fig. S9 n_w is plotted as a function of the pressure Π. Similar curves obtained when the pressure is osmotically applied on a floating bilayer [9] and on multilayer stacks [11] are also presented on Fig. S9. All points follow the same master curve showing that the bilayer behave the same way irrespective how the mechanical stress is applied. This again demonstrates that the floating bilayers keep their integrity under the electric field we apply.
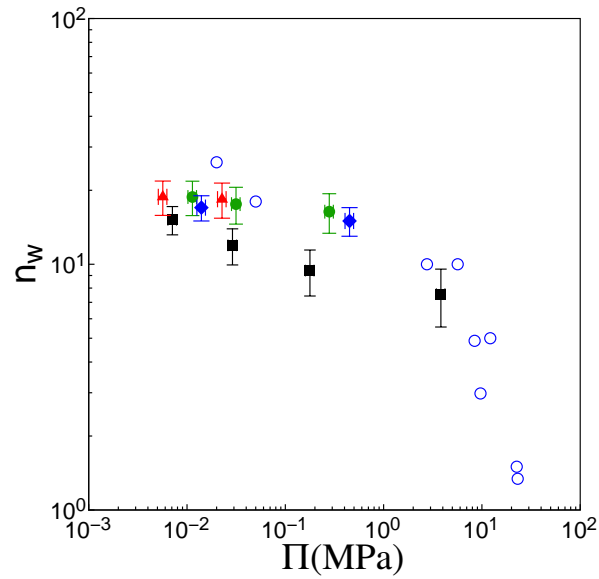

Figure S9: Number of waters per lipid n_w determined from solid-state ^{2}H NMR spectroscopy as a function of osmotic pressure for DMPC multilayer stacks [11] and comparison with our data as a function of electrostatic pressure.

References

[1] F. Ziebert and D. Lacoste. Planar lipid bilayer in an electric field: membrane instability, flow field, and electrical impedance. *Advances in planar lipid bilayers and liposomes, vol. 14*, pages 63–95, 2011.

[2] F. Ziebert and D. Lacoste. Effective zero-thickness model for a conductive membrane driven by an electric field. *New Journal of Physics*, 12:095002, 2010.

[3] William M Haynes. *CRC handbook of chemistry and physics*. CRC press, 2013.

[4] F. Ziebert, M.-Z. Bazant, and D. Lacoste. Effective zero-thickness model for a conductive membrane driven by an electric field. *Physical Review E*, 81:031912, 2010.

[5] T. Charitat, E. Bellet-Amalric, G. Fragneto, and F. Graner. Adsorbed and free lipid bilayers at the solid-liquid interface. *European Physical Journal B*, 8:583–593, 1999.

[6] J. Daillant, E. Bellet-Amalric, A. Braslau, T. Charitat, G. Fragneto, F. Graner, S. Mora, F. Rieutord, and B. Stidder. Structure and fluctuations of a single floating lipid bilayer. *The Proceding of the National Academy of Sciences USA*, 102:11639–11644, 2005.

[7] P. S. Swain and D. Andelman. Supported membranes on chemically structured and rough surfaces. *Physical Review E*, 63:51911, 2001.

[8] L. Malaquin, T. Charitat, Lecuyer S., Fragneto G., and J. Daillant. Controlling interactions in supported bilayers from weak electrostatic repulsion to high osmotic pressure. *Eur. Phys. J. E*, 31(3):285–301, 2010.

[9] Arnaud Hemmerle, Linda Malaquin, Thierry Charitat, Sigolne Lecuyer, Giovanna Fragneto, and Jean Daillant. Controlling interactions in supported bilayers from weak electrostatic repulsion to high osmotic pressure. *Proceedings of the National Academy of Sciences*, 2012.

[10] J.F. Nagle and M.C. Wiener. Relations for lipid bilayers: connections of electron density to other structural quantities. *Mol. Cryst. Liq. Cryst.*, 144:235–255, 1989.

[11] KJ Mallikarjunaiah, Avigdor Leftin, Jacob J Kinnun, Matthew J Justice, Adriana L Rogozea, Horia I Petrache, and Michael F Brown. Solid-state 2 h nmr shows equivalence of dehydration and osmotic pressures in lipid membrane deformation. *Biophysical journal*, 100(1):98–107, 2011.